

Feedback Processes causing an AMOC Collapse in the Community Earth System Model

Elian Vanderborght^a, René M. van Westen^a and Henk A. Dijkstra^{a,b}

^a *Institute for Marine and Atmospheric research Utrecht, Department of Physics, Utrecht
University, Utrecht, the Netherlands*

^b *Centre for Complex Systems Studies, Utrecht University, Utrecht, the Netherlands.*

arXiv:2410.03236v1 [physics.ao-ph] 4 Oct 2024

Corresponding author: Elian Vanderborght, e.y.p.vanderborght@uu.nl

ABSTRACT: The Atlantic Meridional Overturning Circulation (AMOC) is recognized as a tipping element within the global climate system. Central to its tipping behavior is the salt-advection feedback mechanism, which has been extensively studied in box models and models of intermediate complexity. However, in contemporary, highly complex climate models, the importance and functioning of this feedback mechanism is less clear due to the intricate interplay of numerous ocean-atmosphere-sea ice feedbacks. In this study, we conduct a detailed mechanistic analysis of an AMOC collapse under quasi-equilibrium forcing conditions using the Community Earth System Model (CESM). By reconstructing the AMOC strength from the meridional density contrast across the Atlantic Ocean, we demonstrate that AMOC stability can be related to the Atlantic freshwater budget, revealing several important feedbacks. The dominant contribution is the destabilising salt-advection feedback, which is quantified through a negative sign of the overturning freshwater transport at 34°S , indicated by F_{ovs} . Other feedbacks are related to changes in North Atlantic sea-ice melt (destabilising), ocean-atmosphere freshwater fluxes (destabilising) and gyre transports (stabilising). Our study clarifies the role of F_{ovs} as an indicator of the background state stability of the AMOC. As many modern climate models have a positive F_{ovs} bias this implies that their AMOC is too stable which leads to an underestimation of the risk of an AMOC collapse under climate change.

SIGNIFICANCE STATEMENT: The Atlantic Meridional Overturning Circulation (AMOC) is a key component and tipping element in the climate system. Recent climate model simulations demonstrated that the AMOC can tip under the input of freshwater in the Atlantic Ocean. A potential AMOC tipping event has severe climate and societal impacts and it is therefore important to understand the feedback mechanisms that cause the AMOC tipping event. This study identifies and quantifies these feedback mechanisms and their effects on AMOC stability. Our findings show that the dominant salt-advection feedback is responsible for AMOC tipping and is only activated when the AMOC carries net salinity into the Atlantic Ocean. This finding establishes a physical connection between the Atlantic salt transport and the salt-advection feedback. Understanding this connection is important for assessing the risk of AMOC tipping within the 21st century.

1. Introduction

The Atlantic Meridional Overturning Circulation (AMOC) is a part of the global ocean circulation that effectively transports heat, salt and carbon through the Atlantic Ocean (Johns et al. 2011; Broecker 1991). The meridional heat transport by the AMOC plays a significant role in maintaining the temperate climate of Northwestern Europe (Palter 2015). Variations in AMOC strength are also linked to the latitudinal position of the Inter-Tropical Convergence Zone (Schneider et al. 2014) and the Arctic sea-ice extent (Yeager and Robson 2017). Given this important role of the AMOC in the climate system (Rahmstorf 2002; Clark et al. 2002; Zhang et al. 2019), the AMOC is closely monitored along the RAPID-MOCHA measurement array at 26°N since 2004 (Srokosz and Bryden 2015). and shows a time mean (2004 – 2022) strength of 16.9 ± 4.6 Sv ($1 \text{ Sv} \equiv 10^6 \text{ m}^3 \text{ s}^{-1}$). The AMOC is likely to weaken under anthropogenically forced climate change in the remainder of the 21st century (Jackson et al. 2020; Weijer et al. 2020).

The AMOC has been identified as a key tipping element in the climate system (Lenton et al. 2008; Armstrong McKay et al. 2022). This is supported by paleo-climate evidence, showing abrupt climate transitions linked to strong AMOC variations (Dansgaard et al. 1993; de Abreu et al. 2003). Stommel (1961) showed that a highly idealized 2-box model of the AMOC has two stable states under identical freshwater forcing conditions. The emergence of this multi-stable AMOC regime originates from the salt-advection feedback This feedback is characterized by a (North Atlantic) freshwater perturbation that weakens the AMOC, leading to a reduced northward salinity transport and thereby amplifying the initial perturbation (Marotzke 2000).

Rahmstorf (1996) linked the strength of the salt-advection feedback to the freshwater transport carried by the AMOC at the southern boundary (34°S) of the Atlantic Ocean, indicated here by F_{ovS} . This was done in an extended version of the Rooth (1982) box model. When F_{ovS} is positive (negative), the AMOC carries net freshwater (salinity) into the Atlantic Ocean. Huisman et al. (2010) provided a physical link between the F_{ovS} and the salt-advection feedback by constructing an integrated freshwater balance for the Atlantic Ocean and showed that Atlantic freshwater perturbations were only amplified for negative F_{ovS} . This argument provided strong support for F_{ovS} as an indicator for a multi-stable AMOC, where a negative F_{ovS} indicates the existence of a stable collapsed AMOC state under identical freshwater forcing (Sijp 2012).

Building on this theoretical framework, numerous studies employing models of varying complexity confirmed the significance of F_{ovS} as an AMOC stability indicator (de Vries and Weber 2005; Dijkstra 2007; Hawkins et al. 2011; Jackson 2013; van Westen et al. 2024b). Hydrographic observations show that the present-day F_{ovS} is negative (Bryden et al. 2011; Garzoli et al. 2013;

Arumí-Planas et al. 2024) which is in stark contrast with the persistent positive F_{ovS} biases found in the latest generations of climate models (Mecking et al. 2017; van Westen et al. 2024b). The implication would be that climate models underestimate the risk of AMOC tipping under climate change (Jackson 2013; Liu et al. 2017). This results in (unrealistically) high tipping thresholds (e.g., enhanced Greenland Ice Sheet melt and global warming) which are likely not reached within the 21st century (Lenton et al. 2008; Armstrong McKay et al. 2022).

Despite the extensive research underscoring the importance of F_{ovS} , key concerns remain regarding its role in AMOC stability (Gent 2018). First, in a steady-state, the Atlantic freshwater budget represents a balance between the surface freshwater flux and the total horizontal freshwater transport. When a freshwater perturbation is introduced in the North Atlantic, this balance is disrupted, and the system evolves toward a new equilibrium. In the case of overturning freshwater transport, this adjustment is influenced by the salt-advection feedback. However, model studies indicate that other feedbacks, such as those due to the gyre freshwater transport, can sometimes exceed the salt-advection feedback (Mecking et al. 2016; Jackson 2013) which can affect AMOC stability (Cimatoribus et al. 2014). Thus, the importance of the salt-advection feedback depends on the relative influence of other feedback processes within the Atlantic freshwater budget (Gent 2018; Weijer et al. 2019). The complex interplay of multiple feedbacks in coupled climate models further complicates the interpretation of F_{ovS} as a stability indicator.

Second, while arguments support the physical relevance of F_{ovS} within the context of the total Atlantic freshwater balance, there is ambiguity in the relation between the Atlantic freshwater balance and AMOC stability in modern climate models (Mecking et al. 2016; Weijer et al. 2019). An alternative approach to the total Atlantic freshwater balance is by analysing the meridional density (or buoyancy) contrast between the North Atlantic and more southern latitudes. The AMOC responses were successfully reconstructed from thermal wind balance when using this meridional density contrast (Butler et al. 2016; Bonan et al. 2022; Haskins et al. 2019, 2020; Jansen et al. 2018), underlining the importance of the meridional density gradient rather than the total freshwater balance. In this approach, several studies showed that the meridional density gradient was not affected by South Atlantic freshwater transport anomalies (Haines et al. 2022; Cheng et al. 2013; Mignac et al. 2019) challenging the relation between F_{ovS} and the AMOC strength.

The aim of this study is to provide a mechanistic and quantitative description of an AMOC collapse in a modern complex climate model. This mechanistic description addresses the aforementioned points by quantifying the different AMOC feedback strengths and unravels the role of F_{ovS} in AMOC

stability. Thereto we will analyse the recent quasi-equilibrium hosing simulation performed with the Community Earth System Model (CESM) (van Westen and Dijkstra 2023; van Westen et al. 2024b), which shows an AMOC collapse under the slowly increasing freshwater flux forcing. The quasi-equilibrium nature of this simulation provides an ideal case for investigating AMOC feedback mechanisms, enabling us to demonstrate how these feedbacks strengthen or weaken under varying hosing intensities. Our study is organized as follows: Section 2 briefly describes the CESM setup, and introduces the AMOC diagnostics used. Section 3 presents the results using this diagnostic, while Section 4 provides the analysis and interpretation of the findings. Finally, Section 5 provides a summary and discussion.

2. Methods

a. Model

We analyse the simulation presented in van Westen et al. (2024b), performed with the CESM (version 1.0.5. in the f19 g16 configuration). The CESM has a 1° ocean (Parallel Ocean Program version 2, POP2 (Smith et al. 2010)), a 1° sea-ice model (Community Ice Code version 4, CICE4 (Hunke et al. 2010)), and a 2° atmosphere/land component (Community Atmosphere Model version 4, CAM4 (Neale et al. 2013)). Upon initialization from a spin-up solution (Baatsen et al. 2020), the CESM is well equilibrated and the pre-industrial greenhouse forcing conditions are kept constant. The standard monthly-averaged output is converted to yearly averages.

The hosing (i.e., freshwater flux into the ocean) is applied over the Atlantic Ocean between 20°N and 50°N. To conserve salinity, the applied surface freshwater flux is compensated globally elsewhere. The freshwater flux forcing, F_H , linearly increases at a rate of 3×10^{-4} Sv yr⁻¹, similar to Hu et al. (2012). This is a slow hosing rate ensuring quasi-equilibrium conditions, i.e., the CESM stays relatively close to its (statistical) equilibria (van Westen et al. 2024a).

b. Reconstructing the AMOC strength from the buoyancy field

The meridional overturning streamfunction is given by:

$$\psi(t, y, z) = - \int_{-H}^z \left[\int_{x_W}^{x_E} v(t, x, y, z') dx \right] dz' \quad (1)$$

where v is the meridional velocity, H is the water column depth and x_E and x_W refer to the western and eastern boundary of the Atlantic Ocean, respectively. Following Butler et al. (2016), the interior overturning streamfunction, $\psi_{\text{int}}(t, z)$, is defined as $\max\{\psi(t, y, z) \mid y \in [0^\circ\text{N}, 30^\circ\text{N}]\}$.

To analyse the different AMOC feedbacks, we aim to reconstruct the AMOC strength using thermal wind balance (TWB). Specifically, the zonally-integrated meridional velocity V , is in TWB with the zonal basin-scale potential density difference $\Delta_x\rho$ (east minus west) (Cessi and Wolfe 2009). This relation can be expressed as:

$$\frac{\partial V}{\partial z} = \frac{g}{\rho_0 f} \Delta_x \rho, \quad (2)$$

where g is the gravitational acceleration ($= 9.81 \text{ m s}^{-2}$), ρ_0 is a reference density ($= 1025 \text{ kg m}^{-3}$), f is the Coriolis parameter. Physical arguments from Marotzke (1997) and Kuhlbrodt et al. (2007) explain how $\Delta_x\rho$, translates into a basin-scale meridional potential density gradient. Specifically, this relation is given by $\Delta_x\rho = C\Delta_y\rho$, where the dimensionless proportionality constant C incorporates the effects of basin geometry and boundary layer structure (Gnanadesikan 1999).

By combining Equations (1) and (2), we evaluate the TWB overturning transport as:

$$\frac{\partial^2 \hat{\psi}_{\text{int}}}{\partial z^2} = \frac{gC}{\rho_0 f} \Delta_y \rho(z), \quad (3)$$

where the hat superscript refers to the TWB assumption. Equation (3) is solved with the boundary conditions $\hat{\psi}_{\text{int}}(t, 0) = 0 \text{ Sv}$ at the surface and $\hat{\psi}_{\text{int}}(t, -H) = 0 \text{ Sv}$ at the bottom of the ocean. In this way, we reconstruct $\psi_{\text{int}}(t, z)$, as simulated in the CESM, from the buoyancy field by assuming that the AMOC is in TWB (Nikurashin and Vallis 2012). We define $\Psi_{\text{int}}(t) = \psi_{\text{int}}(t, z_{\text{int}})$ (or equivalently $\hat{\Psi}_{\text{int}}(t) = \hat{\psi}_{\text{int}}(t, z_{\text{int}})$) as the (reconstructed) interior AMOC strength, taking $z_{\text{int}} = -1000 \text{ m}$ because $\psi_{\text{int}}(t, z)$ has a maximum around 1,000 m depth.

The buoyancy reconstructed interior streamfunction $\hat{\psi}_{\text{int}}$ and AMOC strength $\hat{\Psi}_{\text{int}}$ depend on both the shape of the density profile and the magnitude of the density contrast (Butler et al. 2016). Hence, we decompose the density contrast as $\Delta_y\rho(z) = \langle \Delta_y\rho \rangle + \gamma(z)$, where $\langle \Delta_y\rho \rangle$ is the vertically-averaged meridional potential density difference, and $\gamma(z)$ represents the deviations from this vertical average. Given this decomposition, changes in the reconstructed AMOC strength are given as:

$$\delta \hat{\Psi}_{\text{int}} = \delta \{ \hat{\Psi}_{\text{int}} \}_{\langle \Delta_y \rho \rangle} + \delta \{ \hat{\Psi}_{\text{int}} \}_{\gamma}, \quad (4)$$

where $\delta \hat{\Psi}_{\text{int}} = \hat{\Psi}_{\text{int}}(t_2) - \hat{\Psi}_{\text{int}}(t_1)$, with t_1 and t_2 denoting two consecutive time instances. The notation $\delta \{F\}_G$ denotes the change in F resulting from a change in G . We later compute the

cumulative change in F , resulting from a change in G , as:

$$\{F\}_G(t) = \sum_{t_i=0}^{t \leq t_i} \delta\{F\}_G(t_i), \quad (5)$$

where t_i denotes the discrete time instances in the model simulation.

The first term on the right hand side of (4) represents the change in Ψ_{int} due to variations in the vertically-averaged potential density contrast, which can be expressed as:

$$\delta\{\hat{\Psi}_{\text{int}}\}_{\langle\Delta_y\rho\rangle} = \frac{gC}{\rho_0 f} D^2 \delta\langle\Delta_y\rho\rangle, \quad (6)$$

where $D^2 = 1/2(-z_{\text{int}}H - z_{\text{int}}^2)$, reflecting the chosen depth for $\hat{\Psi}_{\text{int}}$. The expression for D^2 is found when solving equation (3) with the appropriate boundary conditions, and with $H \approx 4,700$ m we find $D \approx 1,300$ m. The second term on the right hand side in Equation (4), $\delta\{\hat{\Psi}_{\text{int}}\}_\gamma$, accounts for changes in $\hat{\Psi}_{\text{int}}$ due to modifications in the vertical structure of the meridional density contrast profile and consequently quantifies the effect of changes in stratification on the interior AMOC strength.

The vertically-averaged meridional potential density differences (Equation 4) can be further decomposed into a salinity (S) and potential temperature (T) contribution. Specifically, employing a linear equation of state we write:

$$\delta\{\hat{\Psi}_{\text{int}}\}_{\langle\Delta_y\rho\rangle} \approx \frac{gCD^2}{f} (\beta\delta\langle\Delta_y S\rangle - \alpha\delta\langle\Delta_y T\rangle) = \delta\{\hat{\Psi}_{\text{int}}\}_{\langle\Delta_y S\rangle} + \delta\{\hat{\Psi}_{\text{int}}\}_{\langle\Delta_y T\rangle} \quad (7)$$

Here, $\langle\Delta_y T\rangle$ and $\langle\Delta_y S\rangle$ denote the vertically-averaged meridional temperature and salinity contrasts, respectively. The coefficients α ($= 1.3 \times 10^{-4} \text{ K}^{-1}$) and β ($= 7.6 \times 10^{-4} \text{ g}^{-1} \text{ kg}$) are determined by regressing $\delta\{\langle\Delta_y\rho\rangle\}_{\langle\Delta_y T\rangle}$ and $\delta\{\langle\Delta_y\rho\rangle\}_{\langle\Delta_y S\rangle}$ onto $\delta\langle\Delta_y T\rangle$ and $\delta\langle\Delta_y S\rangle$, respectively. The errors introduced by using a linear equation of state are evaluated by computing $\delta\{\hat{\Psi}_{\text{int}}\}_{\langle\Delta_y\rho\rangle} - (\delta\{\hat{\Psi}_{\text{int}}\}_{\langle\Delta_y S\rangle} + \delta\{\hat{\Psi}_{\text{int}}\}_{\langle\Delta_y T\rangle})$, which were verified to be negligible (≤ 0.1 Sv).

c. Freshwater and Heat balance

The drivers of temperature and salinity variations affecting the AMOC strength are analyzed using a heat and freshwater budget analysis. For an arbitrary Atlantic sector, \mathcal{A} (bounded by

latitudes y_1 and y_2), the freshwater and heat balance equations are (Drijfhout et al. 2011):

$$\frac{dW}{dt} = \Delta F_{\text{ov}} + \Delta F_{\text{az}} + F_{\text{res}} + F_{\text{surf}} \quad (8a)$$

$$\frac{d\text{OHC}}{dt} = \Delta Q_{\text{ov}} + \Delta Q_{\text{az}} + Q_{\text{res}} + Q_{\text{surf}} \quad (8b)$$

Here, W and OHC represent the volume-integrated freshwater and ocean heat content over the Atlantic sector \mathcal{A} . The operator Δ denotes the difference in horizontal freshwater and heat transport between the southern (y_1) and northern (y_2) boundaries of \mathcal{A} .

The terms F_{ov} (Q_{ov}) and F_{az} (Q_{az}) represent the freshwater (heat) transport by the overturning and gyre circulation, respectively. They are defined as:

$$F_{\text{ov}}(y) = -\frac{1}{S_0} \int_{-H}^0 \left[\int_{x_{\text{W}}}^{x_{\text{E}}} v^* dx \right] (\hat{S} - S_0) dz, \quad F_{\text{az}}(y) = -\frac{1}{S_0} \int_{-H}^0 \left[\int_{x_{\text{W}}}^{x_{\text{E}}} v' S' dx \right] dz. \quad (9a)$$

$$Q_{\text{ov}}(y) = c_p \rho_0 \int_{-H}^0 \left[\int_{x_{\text{W}}}^{x_{\text{E}}} v^* dx \right] \hat{T} dz, \quad Q_{\text{az}}(y) = c_p \rho_0 \int_{-H}^0 \left[\int_{x_{\text{W}}}^{x_{\text{E}}} v' T' dx \right] dz. \quad (9b)$$

where v^* represents the difference between the zonally-averaged (hatted quantities) and section-averaged velocity, primed quantities indicate deviations from the zonal averages. The constant c_p is the specific heat capacity of seawater ($4186 \text{ J kg}^{-1} \text{ K}^{-1}$) and S_0 is a reference salinity set to 35 g kg^{-1} .

The terms F_{surf} and Q_{surf} represent the area-integrated surface freshwater and heat fluxes for the Atlantic sector, \mathcal{A} . In the CESM, $F_{\text{surf}} = P - E + R + I + M + F_H$ accounts for precipitation (P), evaporation (E , directed to the atmosphere), land run-off (R), ice (I), sea-ice melt and formation (M), and the imposed hosing surface freshwater flux (F_H). Similarly, $Q_{\text{surf}} = SW + LW + SH + LH + MH$ includes short-wave radiation (SW), long-wave radiation (LW), latent heat flux (LH), sensible heat flux (SH), and heat flux due to sea-ice melting and freezing (MH). When $Q_{\text{surf}} < 0$, the heat flux is directed from the ocean to the atmosphere. Any contributions from mixing, barotropic transport, and diffusion are considered as the residual freshwater flux (F_{res}) and residual heat flux (Q_{res}).

3. Result

a. Reconstructing the AMOC

To reconstruct the interior AMOC streamfunction, we require a precise definition of $\Delta_y \rho$ (Equation (3)). In our study, $\Delta_y \rho(z) = \rho_n(z) - \rho_s(z)$ is defined as the meridional density difference

between the North Atlantic (ρ_n) and the South Atlantic (ρ_s), with the latter potentially including parts of the Southern Ocean. The region in the North Atlantic that is crucial in determining AMOC strength lies within the latitude range where isopycnals, shared with the Antarctic Circumpolar Current (ACC), outcrop, and water mass transformation occurs (Nikurashin and Vallis 2012; Wolfe and Cessi 2011). In the CESM, this region is bounded by the latitude range 43°N — 65°N (Figure 1), with $\rho_n(z)$ calculated as the area-averaged potential density within this band. Our results remain robust with slight variations in the latitude range of ρ_n , which aligns with previous studies (Bonan et al. 2022; Jansen et al. 2018).

There is no consensus on the optimal latitude range for ρ_s (Haskins et al. 2019, 2020; Bonan et al. 2022; Butler et al. 2016) and here we aim to optimize the quality of the AMOC reconstruction by selecting a latitude range for ρ_s that effectively captures the relative change in AMOC strength through the thermal wind balance. This optimal reconstruction is achieved when $\rho_s(z)$ is computed as the area-averaged potential density from 56°S to 34°S, and zonally between 53°W and 20°E. The significance of this region is supported by physical arguments presented in Wolfe and Cessi (2010) and Nikurashin and Vallis (2011), showing that the Atlantic interior stratification, in the adiabatic limit, is predominately influenced by processes in the Southern Ocean. Furthermore, in the context of AMOC stability, Wolfe and Cessi (2015) and Cimatoribus et al. (2014) highlight the relevance of outcropping isopycnals in the Southern Ocean. The chosen latitude range for ρ_s captures the outcropping of overlapping isopycnals in the ACC (Figure 1a).

Figure 1b shows the time-mean density contrast ($\Delta_y \rho(z)$) in the first 100 model years. Over the upper 2,000 m, the water mass is denser ($\Delta_y \rho(z) > 0$) in the North Atlantic compared to the South Atlantic. This positive density difference, drives a northward flow in the upper layers (equation (3)). There is hardly any density difference below 2,000 m depths.

The dimensionless proportionality constant C is determined by regressing the model-derived interior streamfunction (Ψ_{int}) onto the TWB reconstruction ($\hat{\Psi}_{\text{int}}$) yielding $C = 0.6$. Figure 2a shows the time-mean profile of the buoyancy reconstructed AMOC strength $\hat{\psi}_{\text{int}}$ for the first 100 model years and the value of ψ_{int} directly determined from the CESM. The TWB reconstruction reasonably captures the upper 1,000 m structure of ψ_{int} . The ψ_{int} maximum is found at 950 m and the TWB reconstructed maxima is found 80 m lower. Below 1,000 m, ψ_{int} rapidly declines towards a -1 Sv near the bottom. This residual corresponds to the Bering Strait volume transport (Jüling et al. 2020). The rapid decline is underestimated by $\hat{\psi}_{\text{int}}$, a discrepancy that arises due to the relatively large density differences between ρ_n and ρ_s below 1,000 m. Additionally, $\hat{\psi}_{\text{int}}$ is zero

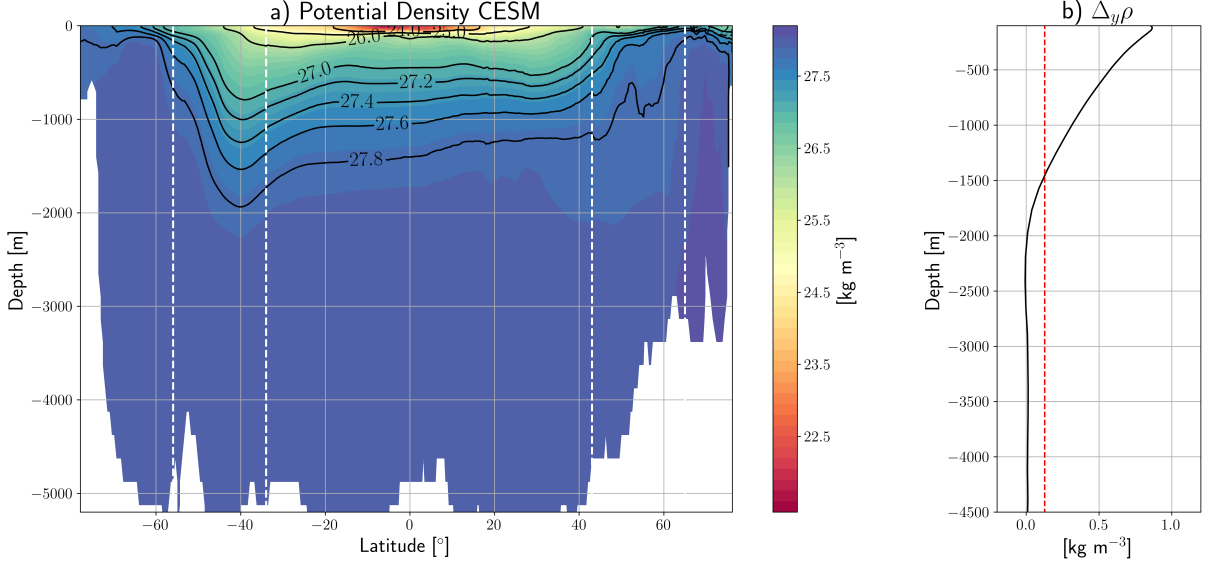


FIG. 1. (a): Time-mean and zonally-averaged potential density of the Atlantic Ocean (full zonal extent) and Southern Ocean (zonal extent between $53^{\circ}\text{W} - 20^{\circ}\text{E}$), for the first 100 model years. (b): Time-mean meridional potential density with depth ($\Delta_y\rho$ thick black) and vertical average ($\langle\Delta_y\rho$) dashed red).

at the bottom (boundary conditions) and does not account for the volume transport through the Bering Strait.

Figure 2b shows the AMOC strength $\hat{\Psi}_{\text{int}}(t)$ and $\Psi_{\text{int}}(t)$ over the complete simulation. As reported by van Westen et al. (2024b), the AMOC strength diminishes with increasing freshwater hosing, with the AMOC tipping event around $F_H = 0.53$ Sv (around model year 1758). The AMOC displays significant variability in the first 500 years of hosing. van Westen et al. (2024b) attributed this to natural variability, but it may also be influenced by the imposed forcing (Ehlert and Levermann 2014). The TWB reconstruction accurately captures the AMOC response to the hosing forcing, including multi-centennial variability, the extent of AMOC weakening due to hosing (approximately 17 Sv), the AMOC tipping event, and the stabilization of the collapsed AMOC. This accurate TWB reconstruction of the collapsed AMOC is achieved only when ρ_s is computed south of the Atlantic basin boundary (34°S), underlining the crucial role of Southern Ocean density stratification in AMOC stability (Wolfe and Cessi 2015). However, some inaccuracies in the TWB reconstruction are notable: it slightly overestimates the rate of AMOC weakening and indicates that the AMOC off-state maintains a northward volume transport of 2.5 Sv.

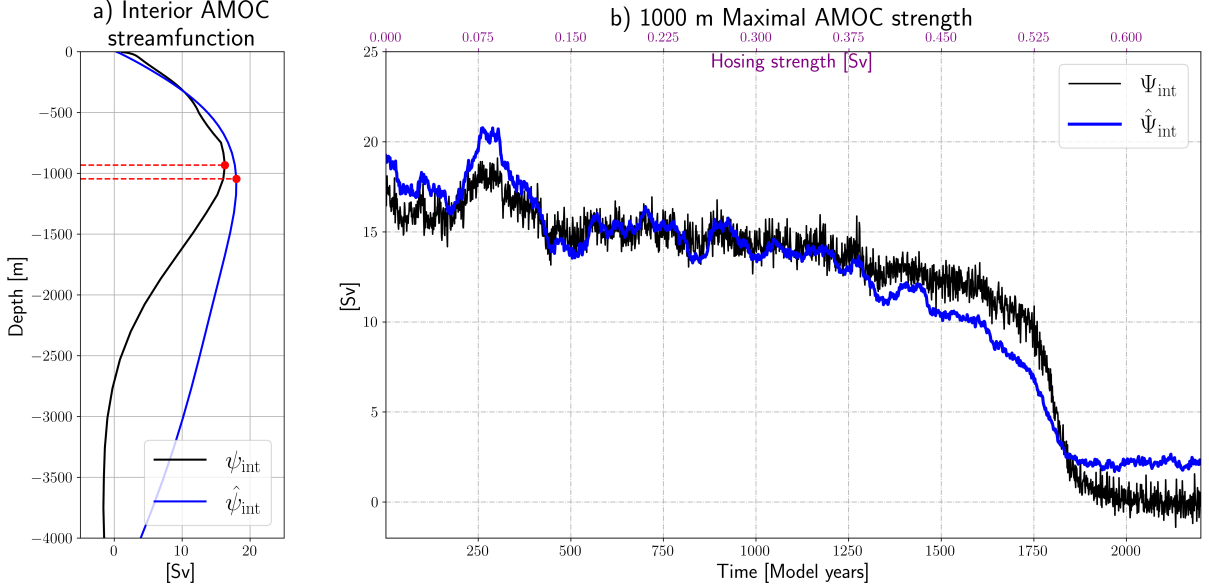


FIG. 2. (a): Time-mean depth dependence of the interior overturning streamfunction (black curve) and TWB reconstruction (blue curve) over the first 100 model years. (b): Interior AMOC strength at 1,000 m under varying hosing strengths F_H , as simulated by the CESM (thick black curve) and the TWB reconstruction (thick blue curve).

b. Attributing changes in AMOC strength

Given that the TWB reconstructed AMOC strength $\hat{\Psi}_{\text{int}}$ provides a reliable estimate for Ψ_{int} , we can interpret changes in AMOC strength as primarily resulting from changes in the basin-scale meridional potential density contrast, $\Delta_y \rho(z)$. Applying Equation (4), we decompose AMOC changes into components related to the vertically-averaged potential density field (i.e. $\delta\{\Psi_{\text{int}}\}_{\langle\Delta_y \rho\rangle}$) and to variations in stratification (i.e., $\delta\{\Psi_{\text{int}}\}_{\gamma}$). The vertically-averaged density contrast is responsible for an AMOC weakening of approximately 20 Sv (Figure 3). Changes in γ contribute to a minor AMOC strengthening of about 3 Sv, which can be attributed to the deepening of the pycnocline. Changes in the vertically-averaged potential density contrast (see inset Figure 3) are therefore dominating the AMOC decline, and the contribution by $\delta\{\Psi_{\text{int}}\}_{\gamma}$ is opposite and much smaller. Notably, $\langle\Delta_y \rho\rangle$ approaches zero when the AMOC collapses which is consistent with results from box models (Stommel 1961; Rahmstorf 1996; Cimadoribus et al. 2014).

We further decompose AMOC changes by a salinity ($\langle\Delta_y S\rangle = \langle S_n - S_s \rangle$) and temperature ($\langle\Delta_y T\rangle = \langle T_n - T_s \rangle$) contribution in Figure 4a, showing $\{\hat{\Psi}_{\text{int}}\}_{\langle\Delta_y S\rangle}$ and $\{\hat{\Psi}_{\text{int}}\}_{\langle\Delta_y T\rangle}$, respectively. Under the increasing freshwater flux forcing, a declined vertically-averaged salinity contrast is weakening the AMOC ($\{\hat{\Psi}_{\text{int}}\}_{\langle\Delta_y S\rangle}$), while temperature variations ($\{\hat{\Psi}_{\text{int}}\}_{\langle\Delta_y T\rangle}$) cause an opposite AMOC response which is approximately half the magnitude of the salinity-driven decrease. Between

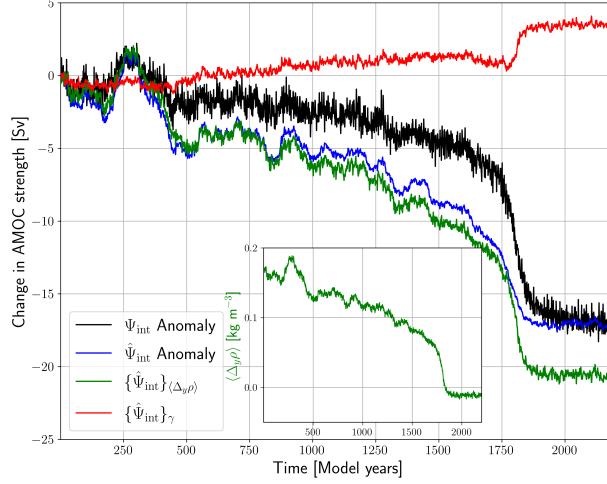


FIG. 3. Decomposition of change in $\hat{\Psi}_{\text{int}}$ (compared to the initial state) driven by changes in vertically-averaged density contrast (thick green line) and stratification (thick red line). Inset shows time series of $\langle \Delta_y \rho \rangle$ (thick green line).

model years 1,800 and 1,900 the contributions reverse and the temperature contrast drives an AMOC decline of 6 Sv while the salinity contrast offsets this decline by about 2 Sv. After model year 2,000, both the salinity and temperature fields stabilize.

Further decomposing the AMOC response into North Atlantic and South Atlantic contributions (Figure 4a), we find that vertically-averaged freshening in the North Atlantic ($\{\hat{\Psi}_{\text{int}}\}_{S_n}$) is the primary driver of the decreasing AMOC strength prior to model year 1,800. Figure 4b shows that this freshening results from an increased surface freshwater flux and freshwater convergence by the overturning circulation. Vertically-averaged cooling of the North Atlantic basin ($\{\hat{\Psi}_{\text{int}}\}_{T_n}$) provides a 50% offset to this decreasing tendency and is related to a decreased overturning heat convergence (Figure 4c), leading to the characteristic AMOC fingerprint (Drijfhout et al. 2012; Caesar et al. 2018).

The AMOC responses induced by the South Atlantic partly offsets the AMOC weakening by the North Atlantic. The main contribution in the South Atlantic comes from vertically-averaged freshening ($\{\hat{\Psi}_{\text{int}}\}_{S_s}$), the vertically-averaged cooling ($\{\hat{\Psi}_{\text{int}}\}_{T_s}$) slightly reduces the AMOC strength. The combined South Atlantic response ($\{\hat{\Psi}_{\text{int}}\}_{\rho_s}$) is +20% (up to the tipping event) compared to the combined North Atlantic response ($\{\hat{\Psi}_{\text{int}}\}_{\rho_n}$), illustrating that North Atlantic salinity changes primarily drive the AMOC decline.

Both the vertically-averaged temperature and salinity over the North Atlantic region increase after model year 1,800. The surface heat flux and heat transport by the gyre drive this ocean heat convergence (Figure 4c), where the former is driven by latent, sensible, and longwave heat fluxes changes in response to an enhanced North Atlantic sea-ice cover (van Westen and Dijkstra 2023).

This temperature increase results in AMOC weakening after model year 1,800 and stabilizes the collapsed AMOC state. The increase in North Atlantic salinity is related to a decreased gyre freshwater convergence and eventually equilibrates with the overturning and surface freshwater fluxes by model year 2,100.

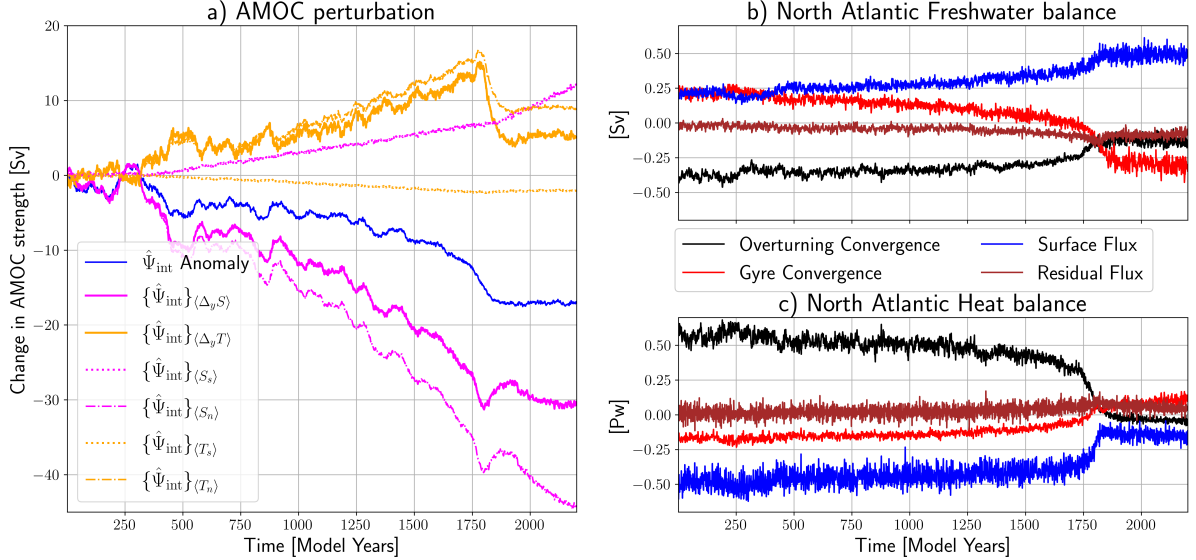


FIG. 4. (a): Decomposition of AMOC perturbations by vertically-averaged potential density changes into thermal (orange) and haline (magenta) by the North (dash-dot) and South Atlantic (dotted). (b & c): The North Atlantic freshwater and heat balances (see equation (8)).

c. AMOC feedbacks: A box-model perspective

We have demonstrated that a realistic AMOC reconstruction can be obtained by using only vertically-averaged quantities. This is analogous to box models where tracer quantities are assumed to be well mixed within each box (Rahmstorf 1996). Therefore, it is tempting to capture the AMOC responses in the CESM with a box model approach and analyse the processes (i.e., salinity) driving the AMOC weakening under the increasing freshwater flux forcing. This will be done by analysing the steady-state Atlantic freshwater budget between 34°S and 65°N (Equation (8a)):

$$0 = F_{\text{surf}} + F_{\text{res}} + (F_{\text{ovS}} - F_{\text{ovN}}) + (F_{\text{azS}} - F_{\text{azN}}). \quad (10)$$

Here, the quantities with a subscript S (N) are evaluated at 34°S (65°N) and the other components are integrated over the Atlantic Ocean surface between 34°S to 65°N.

Given that the AMOC strength at 1,000 m depth at 34°S closely resembles Ψ_{int} (Figure 5a) and considering the negligible contribution of Antarctic Bottom Water (AABW) to F_{ovS} (Van Westen and Dijkstra 2024), we express F_{ovS} as follows (with $\Psi_{\text{int}} > 0$):

$$F_{\text{ovS}} = -\frac{\Psi_{\text{int}}\Delta_v S}{S_0}. \quad (11)$$

where $\Delta_v S$ (determined below) and denotes the velocity-weighted salinity contrast between the northward and southward flowing limbs of the AMOC at 34°S (Sijp 2012). The F_{ovS} sign is now directly related to the $\Delta_v S$ sign. It is important to note that Equation (11) is only valid when a northward overturning state exists, and thus our analysis applies this equation only up to model year 1,850.

In simple box models, the velocity-weighted salinity contrast is simply $\Delta_v S = S_s - S_n$ and assumes that δS_s is uniform throughout the water column (Rahmstorf 1996). This is not the case for the CESM. Specifically, freshwater anomalies originating from the North Atlantic accumulate in the North Atlantic Deep Water (NADW) and are transported southward (quasi-adiabatically) to the South Atlantic (Figure 5b). Hence, it is reasonable to expect that the $\delta\langle S_n \rangle \approx \delta\langle S_l \rangle$, where S_l represents the volume averaged salinity of the South Atlantic NADW. The equilibrated change in South Atlantic salinity can therefore be expressed as:

$$\delta\langle S_s \rangle \approx \frac{\delta\langle S_n \rangle V_l + \delta S_u V_u}{V_s} \quad (12)$$

where $V_s = V_l + V_u$, with V_l representing the volume of the lower limb in the South Atlantic and V_u representing the volume of the upper limb. Here, S_u is the volume-averaged salinity over V_u , representing the Antarctic Intermediate Water (AAIW) and Atlantic Surface Water (ASW). Considering that $\frac{V_u}{V_s} \approx 0.25 - 0.3$ (Figure 5b), it follows that $\delta\Delta_v S = \delta(S_u - \langle S_n \rangle)$. Therefore, we express $\delta\Delta_v\langle S \rangle$ as $-\mu\delta\Delta_v S$, with $\mu \approx 0.25 - 0.3$. We find $\mu = 0.3$ for the CESM (Figure 5c), demonstrating that this approximation and quasi-equilibrium hosing conditions hold. This implies that AMOC responses can be directly related to the vertically-averaged salinity contrast, where we now use $\mu\delta\Delta_v S$ instead of $\delta\Delta_v\langle S \rangle$ (Figure 5d). The $\mu\delta\Delta_v S$ contribution captures the overall AMOC decline prior to the tipping event.

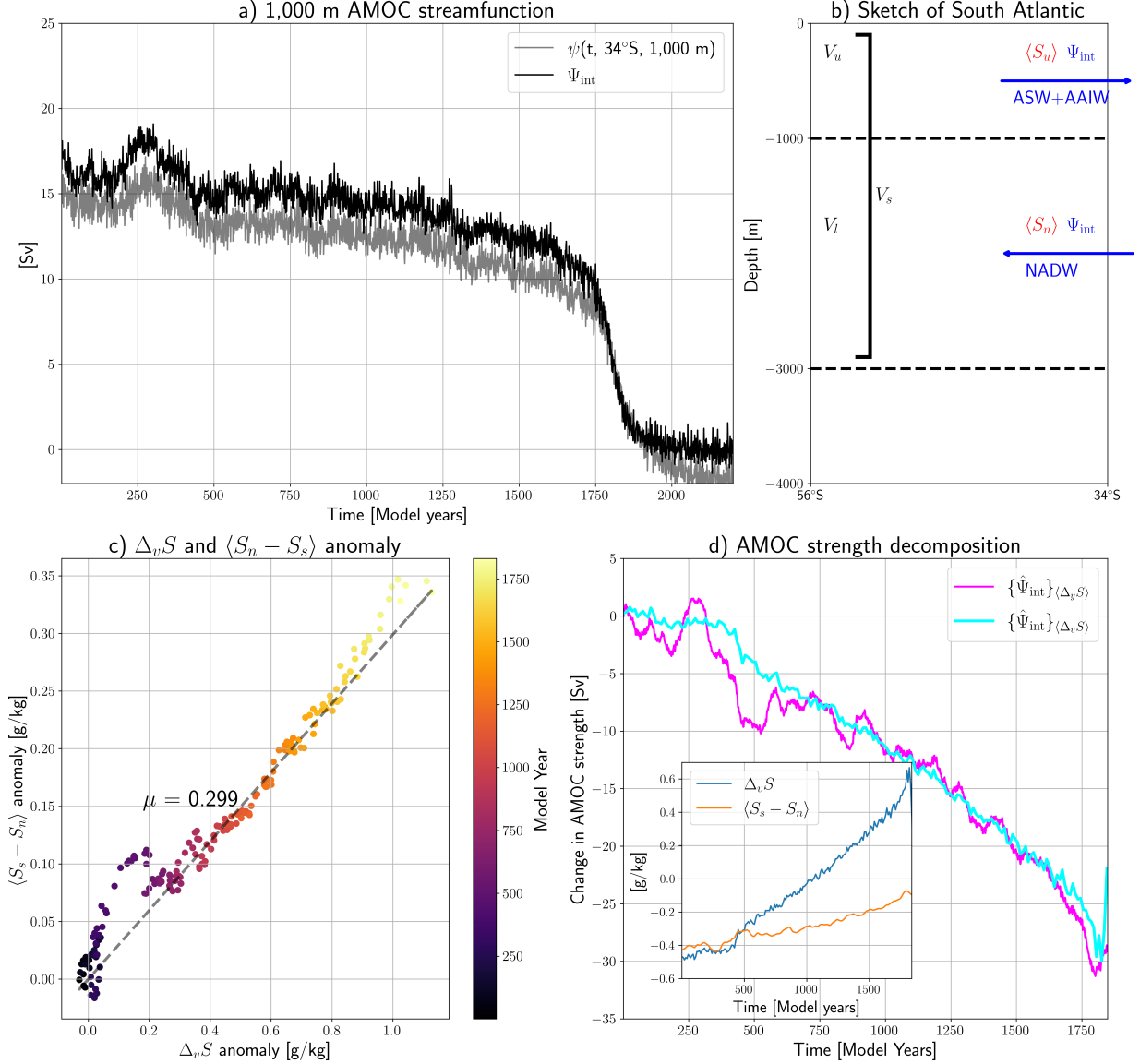


FIG. 5. (a): Interior AMOC streamfunction (thick black) and ψ (equation (1)) evaluated at 34°S and 1,000 depth (thin black). (b): Sketch illustrating the rationale behind equation (12). Arrows indicate the volume transport of the overturning circulation, with the abbreviation below each arrow corresponding to the transported Atlantic water mass. (c): Relation between $\Delta_v S$ and $\langle S_n - S_s \rangle$ anomaly. The slope μ is calculated from a linear regression. Each dot represents a 10-year average. (d): AMOC anomaly resulting from change in $\Delta_v S$ (thick cyan) and $\langle \Delta_y S \rangle$ (thick magenta). Inset shows that time series of $\Delta_v S$ and $\langle S_s - S_n \rangle$.

Applying a small perturbation to the Atlantic freshwater balance (Equation (10)) around a reference state and using Equation (11), we can rewrite it to express $\delta\Delta_v S$ as follows:

$$\delta\Delta_v S = \frac{S_0}{\Psi_{\text{int}}} \left(\delta(F_{\text{azS}} - F_{\text{azN}}) - \delta F_{\text{ovN}} - \frac{1}{S_0} \Delta_v S \delta\Psi_{\text{int}} + \delta F_{\text{surf}} + \delta F_{\text{res}} \right). \quad (13)$$

By combining Equation (7) and (13) we obtain:

$$\begin{aligned} \delta\{\hat{\Psi}_{\text{int}}\}_{\Delta_v S} &\approx \frac{-g\mu S_0 C\beta D^2}{\Psi_{\text{int}f}} \left(\delta(F_{\text{azS}} - F_{\text{azN}}) - \delta F_{\text{ovN}} - \frac{1}{S_0} \delta\Psi_{\text{int}}\Delta_v S + \delta F_{\text{surf}} + \delta F_{\text{res}} \right), \\ &\approx \delta\{\hat{\Psi}_{\text{int}}\}_{\text{Gyre}} + \delta\{\hat{\Psi}_{\text{int}}\}_{\text{ovN}} + \delta\{\hat{\Psi}_{\text{int}}\}_{\text{Saf}} + \delta\{\hat{\Psi}_{\text{int}}\}_{\text{Surf}} + \delta\{\hat{\Psi}_{\text{int}}\}_{\text{Res}} \end{aligned} \quad (14)$$

Terms on the right hand side of Equation (14) quantify the AMOC change resulting from alterations in processes that drive changes in $\Delta_v S$. Specifically, changes in: the gyre freshwater circulation ($\delta\{\hat{\Psi}_{\text{int}}\}_{\text{Gyre}}$), the overturning freshwater transport evaluated at the northern boundary of the Atlantic ($\delta\{\hat{\Psi}_{\text{int}}\}_{\text{ovN}}$), the overturning salt-advection feedback ($\delta\{\hat{\Psi}_{\text{int}}\}_{\text{Saf}}$), the area-integrated surface freshwater flux ($\delta\{\hat{\Psi}_{\text{int}}\}_{\text{Surf}}$), and the residual freshwater flux ($\delta\{\hat{\Psi}_{\text{int}}\}_{\text{Res}}$). It is important to note that contributions from the Atlantic freshwater tendency are neglected in equation (10), leading to a small offset between the left and right hand side of the Equation. Equation (14) demonstrates that AMOC changes, and consequently AMOC stability, are constrained by alterations in the terms of the Atlantic-integrated freshwater balance, as originally proposed by Rahmstorf (1996) and Sijp (2012). Additionally, it highlights that the significance of the overturning salt-advection feedback, amid the presence of other feedbacks, depends on the changes in other components of the freshwater budget (Huisman et al. 2010; Gent 2018).

The different contributions to AMOC changes are shown in Figure 6a and the dominant driver of AMOC weakening is the surface freshwater flux ($\{\hat{\Psi}_{\text{int}}\}_{\text{Surf}}$). As expected, the surface freshwater flux is primarily forced under the increasing hosing strength (Figure 6b). The contribution by hosing is linearly declining up to the AMOC tipping event, but the $\{\hat{\Psi}_{\text{int}}\}_{\text{Surf}}$ decline is non linear after model year 1,200. This non-linear decline is related to additional ocean-atmosphere-sea ice feedbacks, which show a pronounced melt (M) and atmospheric surface freshwater flux ($P - E$) contribution. The contribution by river run-off (R) remains relatively small and ice run-off and brine rejection are negligible (not shown).

Changes in gyre circulation are minimal before model year 1,500, after which they counterbalance the AMOC decline near tipping (Figure 2b), contributing an increase of about 7 Sv from model year 1,000 to 1,750. Similar behavior is noted for $\delta\{\hat{\Psi}_{\text{int}}\}_{\text{Res}}$ and $\delta\{\hat{\Psi}_{\text{int}}\}_{\text{ovN}}$ which offset the AMOC decrease by roughly 3 Sv and 1.5 Sv, respectively, over the same period. The overturning salt-advection feedback ($\{\hat{\Psi}_{\text{int}}\}_{\text{Saf}}$) initially stabilizes the AMOC strength by 2 Sv during the first 1,000 model years. Thereafter, the salt-advection feedback response contributes 6 Sv to AMOC weakening between model year 1,000 to 1,750. The salt-advection feedback, sea-ice melt and ocean-atmosphere fluxes contribute to an accelerated AMOC decline, where the salt-advection

feedback is eventually the most dominant contribution. The precise mechanisms will be further investigated in the next section.

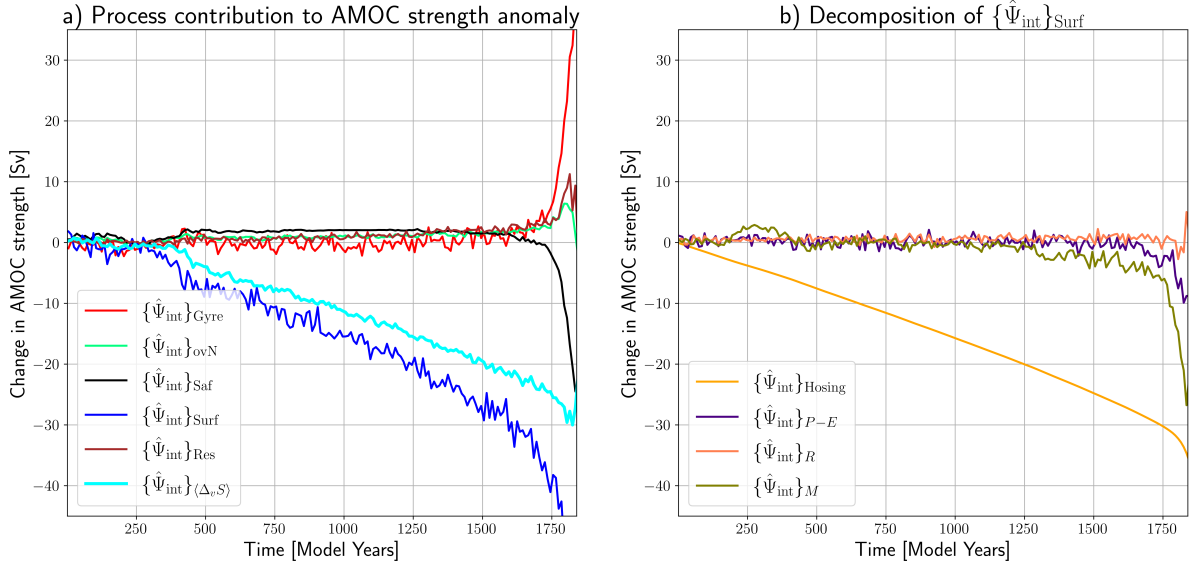


FIG. 6. (a): Contribution of the different terms in equation (14) to the total change in $\{\hat{\Psi}_{\text{int}}\}_{\Delta_{v,S}}$ (cyan line). (b): Decomposition of $\{\hat{\Psi}_{\text{int}}\}_{\text{Surf}}$ into its various components (Melt, P – E, hosing and land run-off). Contributions from ice-runoff are not shown, as they was found to be negligible.

4. Analysis: Feedbacks in the CESM model

a. The Salt-Advection Feedback

The systematic decomposition (14) showed that the overturning salt-advection feedback initially stabilises the AMOC during the first 1,000 model years and contributes to AMOC weakening and the collapse thereafter. In Figure 7a, F_{ovS} is plotted for the complete CESM simulation showing that it changes sign (from positive to negative) around model year 1055 and goes through a minimum just before the collapse. The relation between the salt-advection feedback response ($\delta\{\hat{\Psi}_{\text{int}}\}_{\text{Saf}}$) and the AMOC strength is shown in Figure 7b. When $F_{\text{ovS}} > 0$, a negative AMOC perturbation ($\delta\Psi_{\text{int}} < 0$) is opposed by a positive salt-advection feedback response ($\delta\{\hat{\Psi}_{\text{int}}\}_{\text{Saf}} > 0$). However, when $F_{\text{ovS}} < 0$, a negative AMOC perturbation ($\delta\Psi_{\text{int}} < 0$) is further amplified by the salt-advection feedback response ($\delta\{\hat{\Psi}_{\text{int}}\}_{\text{Saf}} < 0$). The salt-advection feedback strength response becomes stronger (i.e., more negative) for a weaker AMOC. Such a relation between AMOC and F_{ovS} (i.e., salt-advection feedback strength) is also found in the CMIP6 models for the pre-industrial

(1850 – 1899) and present-day (1994 – 2020) period (Van Westen and Dijkstra 2024; van Westen et al. 2024c).

In Appendix A we argue that $\hat{\Psi}_{\text{int}}$ can be approximated as a linear function of $\Delta_v S$, i.e.

$$\hat{\Psi}_{\text{int}}(t) \approx \frac{gCD^2\beta\mu}{f} (a - (1 - c_1) (\Delta_v S(t))), \quad (15)$$

where the constant c_1 represents the efficiency of the overturning thermal advective feedback in mitigating the salinity-driven AMOC decline. As noted earlier, c_1 is approximately 0.5 before tipping occurs (Figure A.1). The parameter a (~ 0.5) is defined in Appendix A and is determined by the equilibrium AMOC strength in the absence of hosing.

Equation (15) enables an explicit evaluation of the salt-advection feedback strength as a function of $\Delta_v S$ (see Appendix A). The resulting expression is:

$$\{\hat{\Psi}_{\text{int}}\}_{\text{Saf}}(t) \approx \frac{g\mu C\beta D^2}{f(1 - c_1)} \left((1 - c_1)(\Delta_v S(t) - \Delta_v S(0)) + a \log \left(\frac{a - (1 - c_1)\Delta_v S(t)}{a - (1 - c_1)\Delta_v S(0)} \right) \right), \quad (16a)$$

$$\frac{\partial \{\hat{\Psi}_{\text{int}}\}_{\text{Saf}}}{\partial \Delta_v S} \approx \frac{g\mu C\beta D^2}{f} \frac{(c_1 - 1)\Delta_v S}{(c_1 - 1)\Delta_v S + a}, \quad (16b)$$

Equation (16b) shows that for $\Delta_v S < 0$ ($F_{\text{ovS}} > 0$), $\delta\{\hat{\Psi}_{\text{int}}\}_{\text{Saf}} > 0$. Conversely, for $\Delta_v S > 0$ ($F_{\text{ovS}} < 0$), $\delta\{\hat{\Psi}_{\text{int}}\}_{\text{Saf}} < 0$. Moreover, for increasing values of $\Delta_v S$ (or F_{ovS}), equation (16b) reveals that the salt-advection feedback becomes logarithmically more effective at weakening the AMOC.

Using equation (15) to rewrite equation (16a) in terms of $\hat{\Psi}_{\text{int}}$, and substituting all necessary parameter values, we obtain an semi-analytic estimate for the salt-advection feedback strength as a function of $\hat{\Psi}_{\text{int}}$ (the dashed curve in Figure 7b). This estimate accurately captures the gradual increase in salt-advection feedback strength as $\Delta_v S$ rises. Despite some assumptions, the framework can recover the gradual AMOC destabilization resulting from the salt-advection feedback and its dependence on the F_{ovS} .

b. Atmospheric and sea-ice AMOC feedbacks

Two additional contributions to the accelerated AMOC decline are the ocean-atmosphere and sea-ice melt surface freshwater fluxes (Figure 6b). Both fluxes increase during the hosing simulation, with sea-ice melt freshwater fluxes increasing by about 0.15 Sv from model year 1 to 1,800, representing a 150% increase from the initial value, in particular after model year 1,200. Atmospheric freshwater fluxes increase by 0.09 Sv (7% increase from initial value), with significant

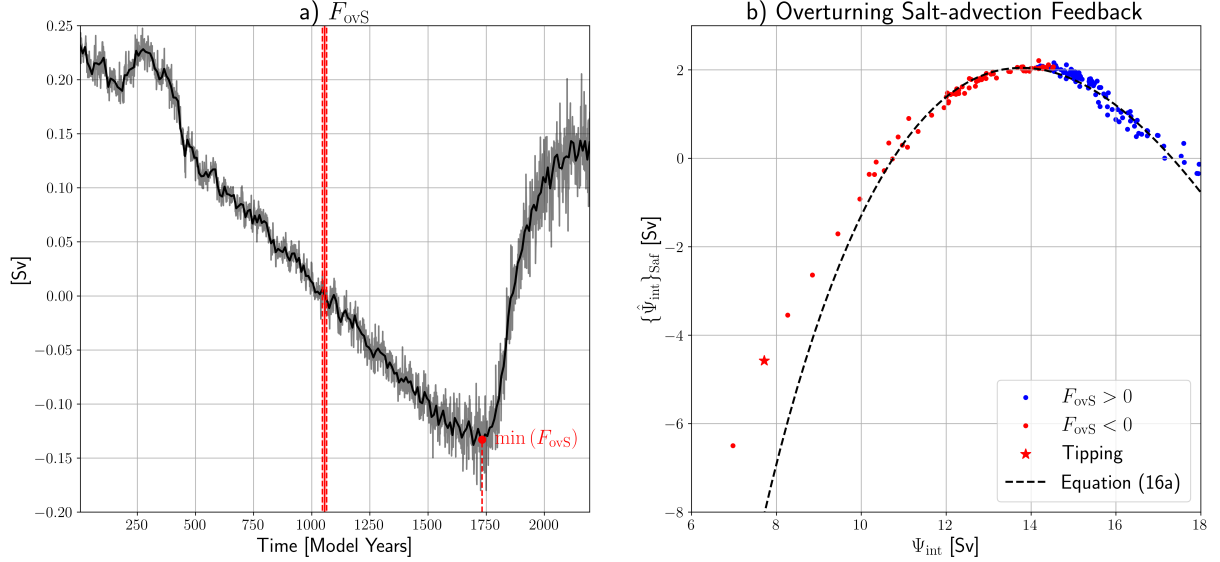


FIG. 7. (a): Time series of F_{ovS} during the hosing simulation (thin black line), along with the 10-year moving average of the same time series (thick black line). The sign of F_{ovS} switches after 1,055 years of hosing (confidence interval: 1,046–1,064 years, 90% confidence, indicated by red shaded bands). The minimum value of F_{ovS} is reached at year 1,732 (confidence interval: 1,727–1,740, 90% confidence) (van Westen et al. 2024b). (b): The relation between $\{\Psi_{\text{int},r}\}_{\text{Saf}}$ and Ψ_{int} for different F_{ovS} signs.

changes emerging after 1,600 model years. The sea-ice melt contribution is correlated with Ψ_{int} , as confirmed by co-integration analysis (Engle and Granger 1987) with a confidence level of $p < 0.01$. No significant co-integration was found between ocean-atmosphere freshwater fluxes and Ψ_{int} .

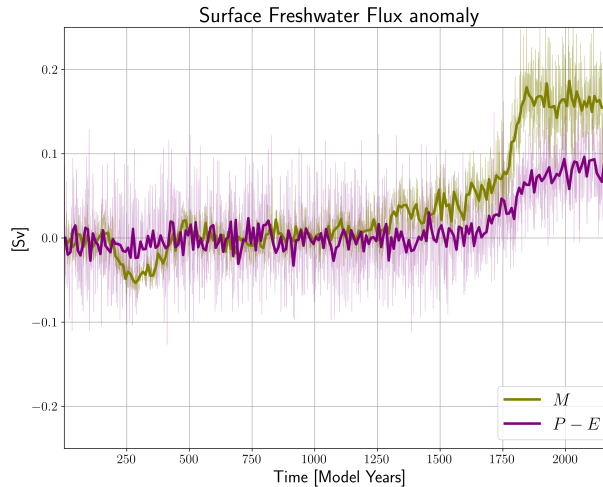


FIG. 8. Time-series of anomalous atmospheric ($P - E$) and sea-ice melt/formation (M) surface freshwater fluxes over the Atlantic Ocean ($34^\circ\text{S} - 65^\circ\text{N}$) in the hosing simulation. Thick lines represent 10-year average of thin lines.

In the CESM, the sea-ice melt freshwater flux can be either negative or positive. When M is negative (during winter), sea-ice formation dominates over sea-ice melt, leading to freshwater

being extracted from the ocean. For positive M (during spring and summer), sea-ice melt exceeds formation, resulting in an influx of freshwater into the ocean surface. The strong correlation between Ψ_{int} and M suggests that a decrease in AMOC strength is associated with a predominant increase in sea-ice melt relative to sea-ice formation over the Atlantic Ocean surface. Figure 9 illustrates the trends in sea-ice formation (Figure 9a) and sea-ice melt (Figure 9b) rates for model years 1,200 to 1,700. In the North Atlantic, the sea-ice formation trend is mostly positive, contributing to a reduction in M . However, consistent with the data shown in Figure 7, the dominant trend is an increase in the melting rate, which results in a net increase in M across the North Atlantic. Approximately 77% of the overall positive trend in the melt rate is attributed to increased basal, lateral, and top melt (not shown), while the remaining 23% is due to heightened snow melt on top of the expanded North Atlantic sea-ice pack.

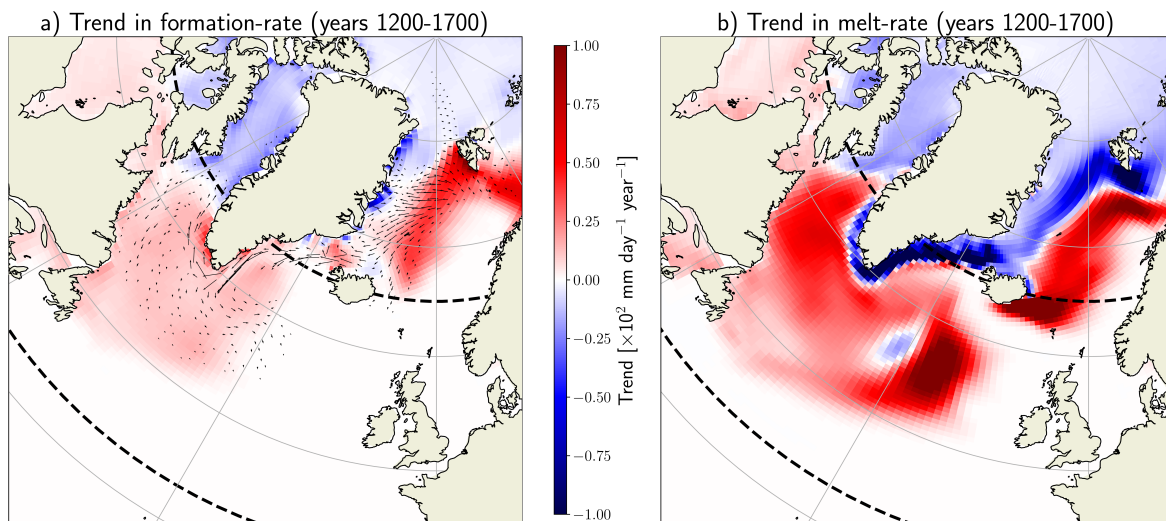


FIG. 9. (a): Tendency of the yearly averaged sea-ice formation rate (colors) and ice transport (arrows) for years 1200 – 1700. (b): Tendency of the yearly averaged melting rate for years 1200-1700. Only significant ($p < 0.05$) trends are shown. Black dashed curves mark the boundaries of the North-Atlantic.

Given the increased net melt of sea ice over the North Atlantic region, it follows that these contributions must originate from outside the region. The sea-ice pack is advected southward from regions north of 65°N (see arrows in Figure 9a). The coastal regions close to south(eastern) boundary of Greenland show negative melt-rate tendencies (lower temperatures due to AMOC weakening), resulting in sea-ice accumulation in the coastal areas. Then, via advection, the sea-ice pack enters the North Atlantic region and during winter time snow accumulates on top of the sea-ice pack. The following spring and summer, the sea-ice pack and snow melt contribute to

a positive growth in M . This sequence of events highlights an AMOC-sea-ice feedback, which further destabilises the AMOC.

The last destabilising AMOC contribution comes from evaporation (Figure 9a) and precipitation (Figure 9b) changes. The most notable changes in evaporation occur in the North Atlantic, where the enhanced sea-ice cover and sea surface cooling lead to a positive (i.e., less negative) evaporation tendency in response to an AMOC strength decline. The cooling effect also results in decreased precipitation over the North Atlantic. However, the evaporation trend dominates, leading to net freshwater into the North Atlantic due to changes in atmospheric fluxes. The opposite precipitation and evaporation responses over the North Atlantic region likely explain the weaker correlation between $P - E$ and Ψ_{int} .

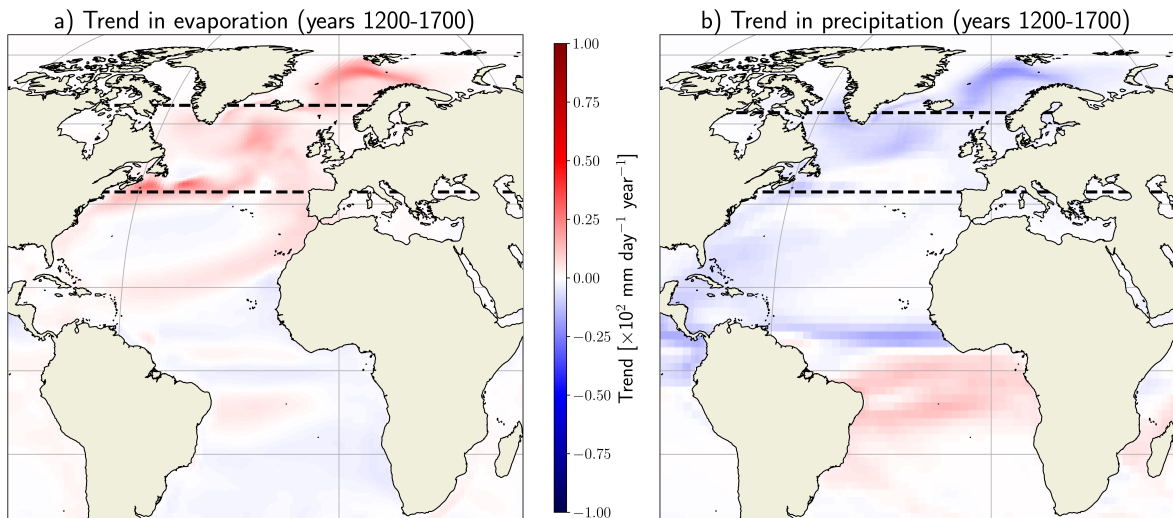


FIG. 10. (a) Tendency of the yearly averaged evaporation rate for years 1000 – 1500. (b) Tendency of the yearly averaged precipitation rate for years 1000-1500. Only significant ($p < 0.05$) trends are shown. Black dashed curves mark the boundaries of the North-Atlantic.

c. Feedbacks from the Gyre circulation

Apart from the three destabilising AMOC contributions, the gyre contribution tends to stabilise the AMOC (Figure 6a). The gyre circulation may modify through changes in the velocity or salinity field (Drijfhout et al. 2011; Weijer et al. 2019). This velocity and salinity decomposition of the gyre freshwater convergence ($F_{\text{azS}} - F_{\text{azN}}$) and the separate contributions from F_{azS} (i.e., freshwater transport by the South Atlantic Subtropical Gyre (SASTG)) and F_{azN} (i.e., freshwater transport by the Subpolar Gyre (SPG)) are shown in Figure 11a. The gyre freshwater convergence

changes are relatively small in the first 1,700 years. Closer to the tipping event, the freshwater convergence decreases and is primarily driven by changes in the salinity field.

Both F_{azN} and F_{azS} increase prior to tipping. This increasing trend is primarily driven by salinity changes, with a dominant salinity decrease at the eastern boundary in the North and South Atlantic (Figure 12a). Following equation (14), the increase in F_{azN} works to stabilize the AMOC decline, while an increasing F_{azS} enhances the AMOC decline (Figure 11b). The contrasting of roles of the SPG and SASTG on AMOC stability before tipping agree with the findings of Cimadoribus et al. (2014), and suggests that the SPG increases (Longworth et al. 2005), while the SASTG decreases the critical freshwater forcing required for AMOC collapse. Consequently, the total effect of the gyres on the critical freshwater forcing is reduced.

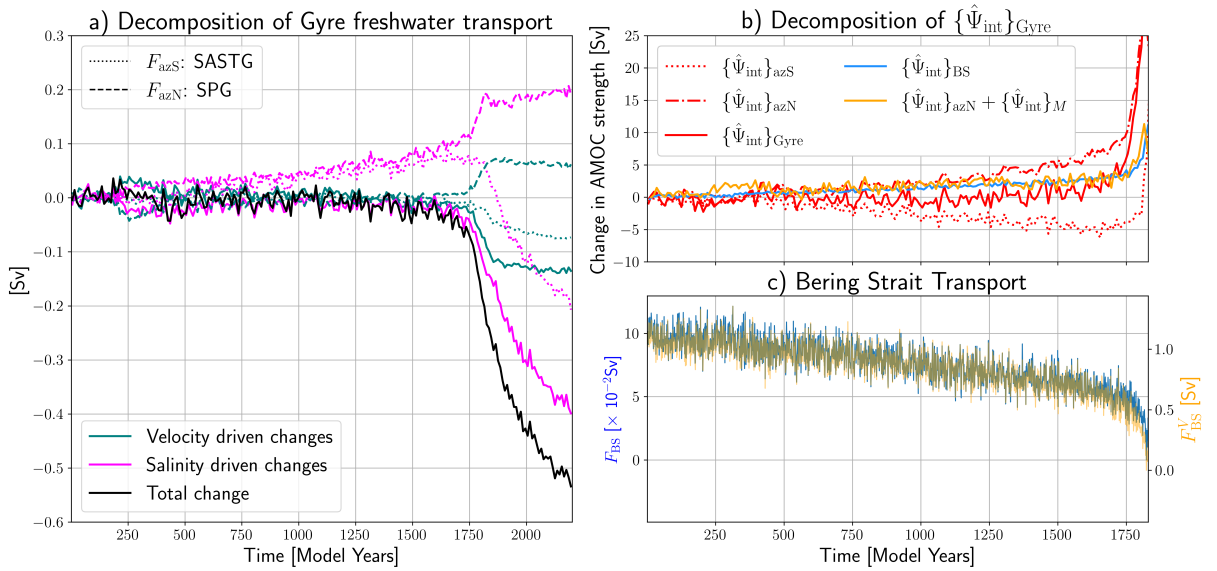


FIG. 11. (a) Decomposition of change in Atlantic gyre freshwater convergence (thick black, $F_{azS} - F_{azN}$) into velocity (thick teal) and salinity (thick magenta). Dotted and dashed line represent decomposition for F_{azS} and F_{azN} , respectively. (b): Contribution of F_{azN} (SPG, dash-dot red), F_{azS} (SASTG, dotted red) and Bering Strait freshwater transport (thick blue line) to change in AMOC strength. The Bering Strait contribution was argued to follow from $-\delta F_{azN} + \delta M \approx \delta F_{BS}$ (Figure 13). (c): Bering Strait freshwater (left y-axis, thick blue line) and volume (right y-axis, thick orange line) transport.

F_{ovS} reaches a minimum (model year 1,732, Figure 7a). This minimum arises as the velocity-induced responses become equally important as the salinity-induced responses, where eventually the velocity-induced responses start to dominate, resulting in a F_{ovS} increase. In other words, the AMOC carries less salinity into the Atlantic Ocean leading to salt accumulation in the southeast Atlantic Ocean (Figure 12b), as also described in Zhu and Liu (2020). This accumulation of salt results in a F_{azS} maximum around the same time as the F_{ovS} minimum. Thereafter, the F_{azS}

declines and contributes to an AMOC stabilisation of about 5 Sv (model years 1,600 – 1,800). This suggests that the SASTG tends to destabilize the northward overturning while also destabilizing the collapsed AMOC, consistent with results from earlier studies (Mecking et al. 2016; Weijer et al. 2019).

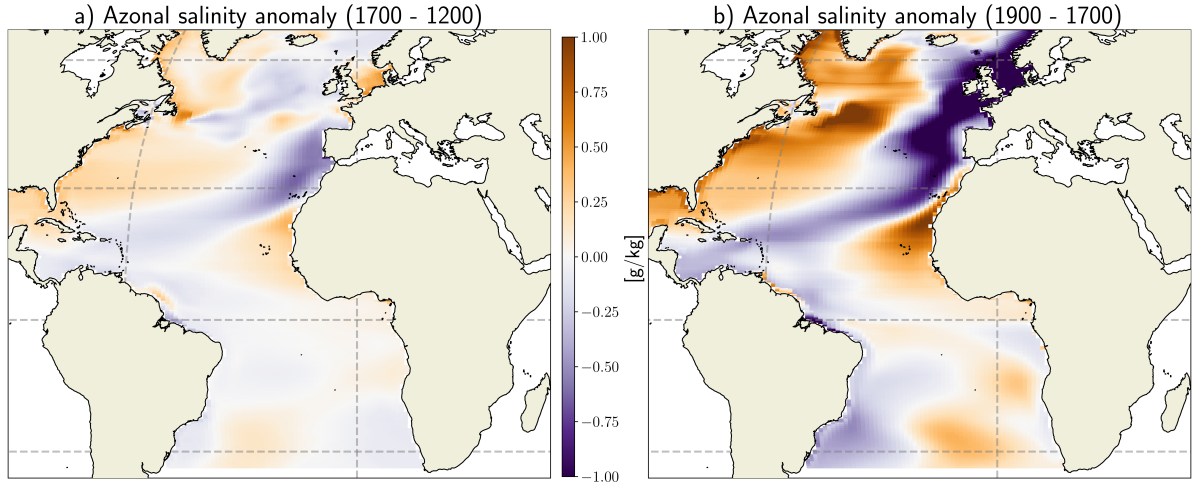


FIG. 12. Vertically-averaged ($\sim 0 - 500$ m) Atlantic Surface water (ASW) azonal salinity difference, with (a): model years 1,700 minus 1,200 and (b) 1,900 minus 1,700.

Figure 13 shows the Arctic Ocean freshwater balance. The salinity influx from the Atlantic Ocean is balanced by a surface freshwater flux and Bering Strait freshwater influx. Under the increasing hosing freshwater flux forcing, the SPG reduces Atlantic salinity influx and this is compensated by a smaller surface freshwater flux and Bering Strait freshwater flux. The surface freshwater flux changes are primarily related to more sea-ice formation, where the sea-ice pack is advected out of the Arctic Ocean and into the North Atlantic (cf. Figure 9). The dominant balance (Figure 13) is then, $\delta F_{azN} + \delta M_{ar} \approx -\delta F_{BS}$, where M_{ar} is the Arctic sea-ice melt freshwater flux which roughly satisfies $\delta M_{ar} \approx \delta M$, with M representing the Atlantic integrated melt surface freshwater flux (cf. Figure 8). According to the framework described above (equation (14)), this balance can be equivalently written as $\delta\{\hat{\Psi}_{int}\}_{azN} + \delta\{\hat{\Psi}_{int}\}_{Melt} \approx \delta\{\hat{\Psi}_{int}\}_{BS}$ (Figure 11b). Hence, the stronger AMOC stabilization of the SPG, relative to the sea-ice melt feedback, can be attributed to the Bering Strait configuration (Hu et al. 2012). Specifically, in the CESM, where the Bering Strait is open, a weakened AMOC results in a decreased northward volume and freshwater transport through Bering Strait (Figure 11c). This increases the Arctic surface salinity and thereby the salt

transport of the southward flowing SPG branch, providing an additional input of salt into the North Atlantic in response to an AMOC weakening.

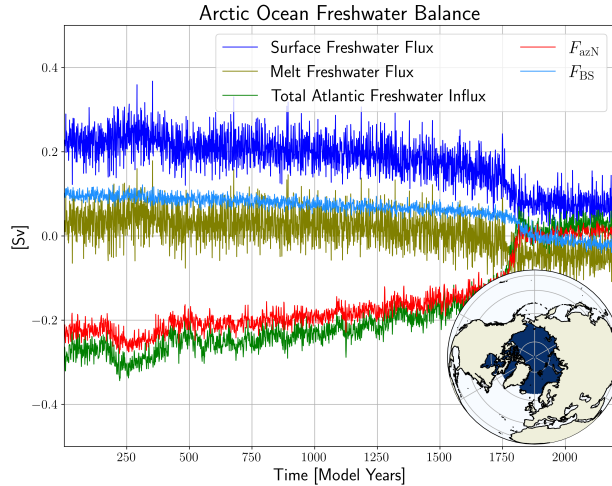


FIG. 13. Arctic freshwater balance (equation (8)). The inset shows the Arctic region (blue).

5. Summary and Discussion

We investigated the feedbacks involved in AMOC tipping within CESM under a quasi-equilibrium hosing (van Westen and Dijkstra 2023), aiming to resolve uncertainties surrounding the role of F_{ovS} as an AMOC stability indicator. Conceptual AMOC box models typically exhibit tipping behavior driven primarily by the salt-advection feedback. In such models, where the density contrast is determined by the Atlantic freshwater budget, F_{ovS} is considered a key indicator of AMOC stability (Rahmstorf 1996). However, modern climate models incorporate a broader range of AMOC feedback mechanisms, complicating the interpretation of F_{ovS} as a single stability metric. Furthermore, unlike box models (Cimatoribus et al. 2014), the link between AMOC stability and the Atlantic freshwater balance in comprehensive climate models is less clear.

Our approach relied on reconstructing the AMOC using the thermal wind balance, a framework strongly supported by theory (Marotzke 1997; Nikurashin and Vallis 2012; Butler et al. 2016). This relation suggests that AMOC strength scales linearly with the twice-vertically-integrated density contrast between the North and South Atlantic. By linking the AMOC strength to the meridional density (or buoyancy) field, we demonstrated that the dominant driver of AMOC weakening is the freshening of the North Atlantic Ocean. The weaker AMOC transports less heat northward, which results in cooling of the North Atlantic Ocean. This cooling stabilises the AMOC as it partially offsets (50%) the AMOC weakening caused by freshening (van Westen et al. 2024a; Rahmstorf

1996). Additional adjustments in the South Atlantic further opposed the AMOC weakening, though their effect was smaller, accounting for a 20% offset.

In analogy to the Rahmstorf (1996) box model, the vertical salinity contrast at 34°S was found to be strongly correlated with the meridional density contrast. Employing thermal wind balance, this correlation allowed us to deduce that AMOC stability can be analyzed from a steady-state Atlantic integrated freshwater balance. Using this framework, we quantified the contributions of various feedback mechanisms that destabilize the northward overturning circulation. The imposed hosing directly weakens the AMOC, but here we focus on the feedbacks that amplify the imposed hosing. The overturning salt-advection feedback is the dominant destabilising mechanism and is responsible for the AMOC collapse. The salt-advection feedback response is related to the F_{ovS} sign. When $F_{\text{ovS}} < 0$, the salt-advection destabilizes the AMOC and the opposite is true for $F_{\text{ovS}} > 0$. Furthermore, the strength of the destabilizing salt-advection feedback increases disproportionately with decreasing F_{ovS} . Our findings are therefore consistent with previous studies (Huisman et al. 2010; Sijp 2012), without relying on the assumption that AMOC stability relates to the Atlantic freshwater content (van Westen et al. 2024b).

In addition to the overturning salt-advection feedback, other destabilizing mechanisms were identified, such as enhanced sea-ice melt and increased atmospheric freshwater flux in response to AMOC weakening. The gyre circulation played a key role in stabilizing the AMOC during hosing, with the subpolar gyre in the North Atlantic providing the primary stabilization. While the subtropical gyre in the South Atlantic contributes to AMOC destabilization, the North Atlantic gyre’s stabilizing effect is dominant. This contrasting influence of the two gyres aligns with box model results from Cimadoribus et al. (2014). The strong stabilization by the North Atlantic subpolar gyre may be linked to the open Bering Strait configuration in CESM. In response to an AMOC decline, this configuration allows additional salt to enter the Arctic Sea, which is then transported to the outcropping region by the gyre’s southward branch, as suggested by Hu et al. (2012). However, we acknowledge that the CESM version analyzed here lacks eddy-resolving dynamics, which have been shown to significantly affect the Atlantic freshwater balance and AMOC stability (Mecking et al. 2016; Toom et al. 2014; Jüling et al. 2020). The contribution of eddies to AMOC stability remains a subject for future investigation.

Shown in Figure 4a, the haline ($\{\hat{\Psi}_{\text{int}}\}_{\langle\Delta_y, S\rangle}$) and thermally driven ($\{\hat{\Psi}_{\text{int}}\}_{\langle\Delta_y, T\rangle}$) AMOC changes display strong opposing variability on a multi-centennial timescale. The origin of this multi-centennial variability has been attributed to the salt-advection feedback (Li and Yang 2022) and its amplitude is damped by the thermal advective overturning feedback (Yang et al. 2024a). Figure

4a shows that this variability originates from vertically-averaged density variations in the North Atlantic, consistent with recent work (Yang et al. 2024b; Cheng et al. 2018). Figure 5d showed that this multi-centennial variability is not captured in the AMOC reconstruction at 34°S ($\{\hat{\Psi}_{\text{int}}\}_{\Delta_{v,S}}$). This suggests that buoyancy anomalies driving the variability remain localized to the North Atlantic. Therefore, they operate independently of the Atlantic freshwater balance, or F_{ovS} . This explains why recent studies (Haines et al. 2022; Cheng et al. 2018; Mignac et al. 2019) found no significant influence of South Atlantic freshwater transport anomalies on AMOC strength under statistically stationary conditions. However, the 34°S AMOC reconstruction does capture the persistent weakening of the AMOC under increasing hosing strength. This implies that adjustments toward a new equilibrium under altered forcing, such as hosing, depend on the Atlantic freshwater budget, particularly F_{ovS} . Specifically, equations (14) and (16) indicate that a more negative F_{ovS} requires a larger decline in AMOC strength for each unit of North Atlantic hosing increase.

Our study provides further evidence that F_{ovS} measures the stability of a (statistically) stationary AMOC state and hence provides a measure of the distance from the critical freshwater forcing threshold (Rahmstorf 1996). While an integrated freshwater budget may not be ideal for assessing stability under rapid transient forcing (e.g., climate change), the initial F_{ovS} value still provides a useful estimate of the AMOC response to buoyancy anomalies (Liu et al. 2017; van Westen et al. 2024c). Since most CMIP5 and CMIP6 models exhibit a positive F_{ovS} (Mecking et al. 2017; Van Westen and Dijkstra 2024), the AMOC in their background climate states is overly stable, leading to an underestimation of the risk of AMOC tipping. It is therefore crucial that the climate models participating in CMIP7 reduce their F_{ovS} biases to better capture AMOC responses to climate change.

Acknowledgments

E.Y.P.V., R.M.v.W. and H.A.D. are funded by the European Research Council through the ERC-AdG project TAOC (project 101055096, PI: Dijkstra). The authors gratefully acknowledge Michael Kliphuis (IMAU, UU) for performing the model simulations presented in this study. The CESM model simulations and the analysis of all the model output was conducted on the Dutch National Supercomputer Snellius within NWO-SURF project 2024.013.

Availability Statement

The analysis scripts will be made available on Zenodo upon publication.

Appendix A: Derivation of Equation (16)

Figure 3 shows that we can approximate the AMOC strength as:

$$\Psi_{\text{int}} \approx \Psi_{\text{int}}(0) + \{\hat{\Psi}_{\text{int}}\}_{\langle \Delta_y, \rho \rangle}, \quad (\text{A.1})$$

From Figure 5, it follows that $\{\hat{\Psi}_{\text{int}}\}_{\langle \Delta_y, T \rangle}$ scales linearly with $-\{\hat{\Psi}_{\text{int}}\}_{\langle \Delta_y, S \rangle}$. This makes sense given that, prior to AMOC tipping, changes in North Atlantic temperature result from the weakening of the overturning circulation, which in turn is linked to the North Atlantic freshening. Therefore, we can express the overturning streamfunction as:

$$\Psi_{\text{int}}(t) \approx \Psi_{\text{int}}(0) + (1 - c_1) \{\hat{\Psi}_{\text{int}}\}_{\langle \Delta_y, S \rangle}(t), \quad (\text{A.2})$$

where the constant c_1 quantifies the efficiency of the thermal advective feedback in offsetting the salinity-driven AMOC decrease. We assume that c_1 is independent of time, which is supported by statistical analysis (Figure A.1).

The linear relation between $\langle \Delta_y, S \rangle$ and $\Delta_v S$ can now be used to express:

$$\{\hat{\Psi}_{\text{int}}\}_{\langle \Delta_y, S \rangle}(t) = -\frac{gCD^2\beta\mu}{f} (\Delta_v S(t) - \Delta_v S(0)). \quad (\text{A.3})$$

Combining equations (A.2) and (A.3), we can rewrite the expression for Ψ_{int} as:

$$\Psi_{\text{int}}(t) \approx \frac{gCD^2\beta\mu}{f} \left(\underbrace{\frac{\Psi_{\text{int}}(0)f}{gCD^2\beta\mu} + (1 - c_1)\Delta_v S(0)}_a - (1 - c_1)\Delta_v S(t) \right). \quad (\text{A.4})$$

Assuming that the time instances t_1 and t_2 are infinitesimally close, $\delta\Psi_{\text{int}}$ becomes $d\Psi_{\text{int}}$. Inserting equation (A.4) into the definition of the salt-advection feedback contribution (equation (14)) and integrating over $\Delta_v S$ we express:

$$\{\hat{\Psi}_{\text{int}}\}_{\text{Saf}} = -\frac{g\mu C\beta D^2(1 - c_1)}{f} \left(\int_{\Delta_v S(0)}^{\Delta_v S(t)} \frac{\Delta_v S'}{a - (1 - c_1)\Delta_v S'} d(\Delta_v S)' \right). \quad (\text{A.5})$$

It then follows:

$$\{\hat{\Psi}_{\text{int}}\}_{\text{Saf}} \approx \frac{g\mu C\beta D^2}{f(1-c_1)} \left((1-c_1)(\Delta_v S(t) - \Delta_v S(0)) + a \log \left(\frac{a - (1-c_1)\Delta_v S(t)}{a - (1-c_1)\Delta_v S(0)} \right) \right). \quad (\text{A.6})$$

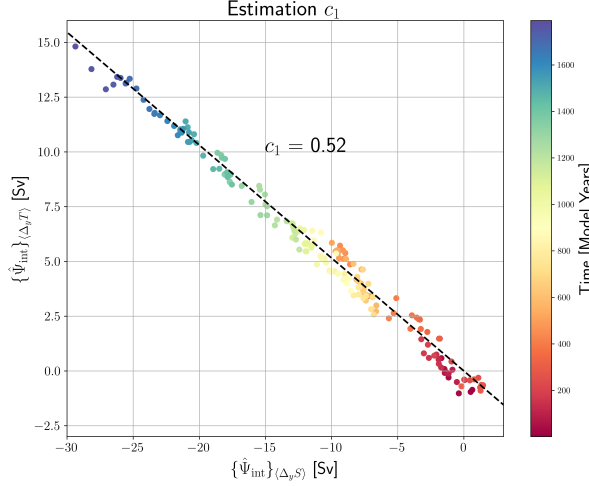


FIG. A.1. Relation between $\{\hat{\Psi}_{\text{int}}\}_{\langle\Delta,S\rangle}$ and $\{\hat{\Psi}_{\text{int}}\}_{\langle\Delta,T\rangle}$, where each dot represents a 10-year average. Slope of relation determines value of $-c_1$.

References

- Armstrong McKay, D. I., and Coauthors, 2022: Exceeding 1.5 c global warming could trigger multiple climate tipping points. *Science*, **377** (6611), eabn7950.
- Arumí-Planas, C., S. Dong, R. Perez, M. J. Harrison, R. Farneti, and A. Hernández-Guerra, 2024: A multi-data set analysis of the freshwater transport by the atlantic meridional overturning circulation at nominally 34.5 s. *Journal of Geophysical Research: Oceans*, **129** (6), e2023JC020 558.
- Baatsen, M., A. S. Von Der Heydt, M. Huber, M. A. Kliphuis, P. K. Bijl, A. Sluijs, and H. A. Dijkstra, 2020: The middle to late eocene greenhouse climate modelled using the cesm 1.0. 5. *Climate of the Past*, **16** (6), 2573–2597.
- Bonan, D. B., A. F. Thompson, E. R. Newsom, S. Sun, and M. Rugenstein, 2022: Transient and equilibrium responses of the atlantic overturning circulation to warming in coupled climate models: The role of temperature and salinity. *Journal of Climate*, **35** (15), 5173–5193.
- Broecker, W. S., 1991: The great ocean conveyor. *Oceanography*, **4** (2), 79–89.

- Bryden, H. L., B. A. King, and G. D. McCarthy, 2011: South atlantic overturning circulation at 24 s. *Journal of Marine Research*, **69** (1), 38–55.
- Butler, E., K. Oliver, J. J.-M. Hirschi, and J. Mecking, 2016: Reconstructing global overturning from meridional density gradients. *Climate Dynamics*, **46**, 2593–2610.
- Caesar, L., S. Rahmstorf, A. Robinson, G. Feulner, and V. Saba, 2018: Observed fingerprint of a weakening atlantic ocean overturning circulation. *Nature*, **556** (7700), 191–196.
- Cessi, P., and C. L. Wolfe, 2009: Eddy-driven buoyancy gradients on eastern boundaries and their role in the thermocline. *Journal of physical oceanography*, **39** (7), 1595–1614.
- Cheng, W., J. C. Chiang, and D. Zhang, 2013: Atlantic meridional overturning circulation (amoc) in cmip5 models: Rcp and historical simulations. *Journal of Climate*, **26** (18), 7187–7197.
- Cheng, W., and Coauthors, 2018: Can the salt-advection feedback be detected in internal variability of the atlantic meridional overturning circulation? *Journal of Climate*, **31** (16), 6649–6667.
- Cimatoribus, A. A., S. S. Drijfhout, and H. A. Dijkstra, 2014: Meridional overturning circulation: stability and ocean feedbacks in a box model. *Climate dynamics*, **42**, 311–328.
- Clark, P. U., N. G. Pisias, T. F. Stocker, and A. J. Weaver, 2002: The role of the thermohaline circulation in abrupt climate change. *Nature*, **415** (6874), 863–869.
- Dansgaard, W., and Coauthors, 1993: Evidence for general instability of past climate from a 250-kyr ice-core record. *nature*, **364** (6434), 218–220.
- de Abreu, L., N. J. Shackleton, J. Schönfeld, M. Hall, and M. Chapman, 2003: Millennial-scale oceanic climate variability off the western iberian margin during the last two glacial periods. *Marine Geology*, **196** (1-2), 1–20.
- de Vries, P., and S. L. Weber, 2005: The atlantic freshwater budget as a diagnostic for the existence of a stable shut down of the meridional overturning circulation. *Geophysical Research Letters*, **32** (9).
- Dijkstra, H. A., 2007: Characterization of the multiple equilibria regime in a global ocean model. *Tellus A: Dynamic Meteorology and Oceanography*, **59** (5), 695–705.
- Drijfhout, S., G. J. Van Oldenborgh, and A. Cimatoribus, 2012: Is a decline of amoc causing the warming hole above the north atlantic in observed and modeled warming patterns? *Journal of Climate*, **25** (24), 8373–8379.

- Drijfhout, S. S., S. L. Weber, and E. van der Swaluw, 2011: The stability of the moc as diagnosed from model projections for pre-industrial, present and future climates. *Climate Dynamics*, **37**, 1575–1586.
- Ehlert, D., and A. Levermann, 2014: Mechanism for potential strengthening of atlantic overturning prior to collapse. *Earth System Dynamics*, **5 (2)**, 383–397.
- Engle, R. F., and C. W. Granger, 1987: Co-integration and error correction: representation, estimation, and testing. *Econometrica: journal of the Econometric Society*, 251–276.
- Garzoli, S. L., M. O. Baringer, S. Dong, R. C. Perez, and Q. Yao, 2013: South atlantic meridional fluxes. *Deep Sea Research Part I: Oceanographic Research Papers*, **71**, 21–32.
- Gent, P. R., 2018: A commentary on the atlantic meridional overturning circulation stability in climate models. *Ocean Modelling*, **122**, 57–66.
- Gnanadesikan, A., 1999: A simple predictive model for the structure of the oceanic pycnocline. *Science*, **283 (5410)**, 2077–2079.
- Haines, K., D. Ferreira, and D. Mignac, 2022: Variability and feedbacks in the atlantic freshwater budget of cmip5 models with reference to atlantic meridional overturning circulation stability. *Frontiers in Marine Science*, **9**, 830 821.
- Haskins, R. K., K. I. Oliver, L. C. Jackson, S. S. Drijfhout, and R. A. Wood, 2019: Explaining asymmetry between weakening and recovery of the amoc in a coupled climate model. *Climate dynamics*, **53**, 67–79.
- Haskins, R. K., K. I. Oliver, L. C. Jackson, R. A. Wood, and S. S. Drijfhout, 2020: Temperature domination of amoc weakening due to freshwater hosing in two gcms. *Climate dynamics*, **54**, 273–286.
- Hawkins, E., R. S. Smith, L. C. Allison, J. M. Gregory, T. J. Woollings, H. Pohlmann, and B. De Cuevas, 2011: Bistability of the atlantic overturning circulation in a global climate model and links to ocean freshwater transport. *Geophysical Research Letters*, **38 (10)**.
- Hu, A., and Coauthors, 2012: Role of the bering strait on the hysteresis of the ocean conveyor belt circulation and glacial climate stability. *Proceedings of the National Academy of Sciences*, **109 (17)**, 6417–6422.

- Huisman, S. E., M. Den Toom, H. A. Dijkstra, and S. Drijfhout, 2010: An indicator of the multiple equilibria regime of the atlantic meridional overturning circulation. *Journal of Physical Oceanography*, **40** (3), 551–567.
- Hunke, E. C., W. H. Lipscomb, A. K. Turner, N. Jeffery, and S. Elliott, 2010: Cice: the los alamos sea ice model documentation and software user’s manual version 4.1 la-cc-06-012. *T-3 Fluid Dynamics Group, Los Alamos National Laboratory*, **675**, 500.
- Jackson, L., 2013: Shutdown and recovery of the amoc in a coupled global climate model: the role of the advective feedback. *Geophysical Research Letters*, **40** (6), 1182–1188.
- Jackson, L. C., and Coauthors, 2020: Impact of ocean resolution and mean state on the rate of amoc weakening. *Climate Dynamics*, **55** (7-8), 1711–1732.
- Jansen, M. F., L.-P. Nadeau, and T. M. Merlis, 2018: Transient versus equilibrium response of the ocean’s overturning circulation to warming. *Journal of Climate*, **31** (13), 5147–5163.
- Johns, W. E., and Coauthors, 2011: Continuous, array-based estimates of atlantic ocean heat transport at 26.5 n. *Journal of Climate*, **24** (10), 2429–2449.
- Jüling, A., X. Zhang, D. Castellana, A. S. Von Der Heydt, and H. A. Dijkstra, 2020: The atlantic’s freshwater budget under climate change in the community earth system model with strongly eddying oceans. *Ocean Science Discussions*, **2020**, 1–30.
- Kuhlbrodt, T., A. Griesel, M. Montoya, A. Levermann, M. Hofmann, and S. Rahmstorf, 2007: On the driving processes of the atlantic meridional overturning circulation. *Reviews of Geophysics*, **45** (2).
- Lenton, T. M., H. Held, E. Kriegler, J. W. Hall, W. Lucht, S. Rahmstorf, and H. J. Schellnhuber, 2008: Tipping elements in the earth’s climate system. *Proceedings of the national Academy of Sciences*, **105** (6), 1786–1793.
- Li, Y., and H. Yang, 2022: A theory for self-sustained multicentennial oscillation of the atlantic meridional overturning circulation. *Journal of Climate*, **35** (18), 5883–5896.
- Liu, W., S.-P. Xie, Z. Liu, and J. Zhu, 2017: Overlooked possibility of a collapsed atlantic meridional overturning circulation in warming climate. *Science Advances*, **3** (1), e1601666.
- Longworth, H., J. Marotzke, and T. F. Stocker, 2005: Ocean gyres and abrupt change in the thermohaline circulation: A conceptual analysis. *Journal of climate*, **18** (13), 2403–2416.

- Marotzke, J., 1997: Boundary mixing and the dynamics of three-dimensional thermohaline circulations. *Journal of Physical Oceanography*, **27** (8), 1713–1728.
- Marotzke, J., 2000: Abrupt climate change and thermohaline circulation: Mechanisms and Predictability. *Proc. Natl. Acad. Sci.*, **97**, 1347–1350.
- Mecking, J., S. Drijfhout, L. Jackson, and M. Andrews, 2017: The effect of model bias on atlantic freshwater transport and implications for amoc bi-stability. *Tellus A: Dynamic Meteorology and Oceanography*, **69** (1), 1299–910.
- Mecking, J., S. S. Drijfhout, L. C. Jackson, and T. Graham, 2016: Stable amoc off state in an eddy-permitting coupled climate model. *Climate Dynamics*, **47**, 2455–2470.
- Mignac, D., D. Ferreira, and K. Haines, 2019: Decoupled freshwater transport and meridional overturning in the south atlantic. *Geophysical Research Letters*, **46** (4), 2178–2186.
- Neale, R. B., J. Richter, S. Park, P. H. Lauritzen, S. J. Vavrus, P. J. Rasch, and M. Zhang, 2013: The mean climate of the community atmosphere model (cam4) in forced sst and fully coupled experiments. *Journal of Climate*, **26** (14), 5150–5168.
- Nikurashin, M., and G. Vallis, 2011: A theory of deep stratification and overturning circulation in the ocean. *Journal of Physical Oceanography*, **41** (3), 485–502.
- Nikurashin, M., and G. Vallis, 2012: A theory of the interhemispheric meridional overturning circulation and associated stratification. *Journal of Physical Oceanography*, **42** (10), 1652–1667.
- Palter, J. B., 2015: The role of the gulf stream in european climate. *Annual review of marine science*, **7**, 113–137.
- Rahmstorf, S., 1996: On the freshwater forcing and transport of the atlantic thermohaline circulation. *Climate Dynamics*, **12**, 799–811.
- Rahmstorf, S., 2002: Ocean circulation and climate during the past 120,000 years. *Nature*, **419** (6903), 207–214.
- Rooth, C., 1982: Hydrology and ocean circulation. *Progress in Oceanography*, **11** (2), 131–149.
- Schneider, T., T. Bischoff, and G. H. Haug, 2014: Migrations and dynamics of the intertropical convergence zone. *Nature*, **513** (7516), 45–53.

- Sijp, W. P., 2012: Characterising meridional overturning bistability using a minimal set of state variables. *Climate dynamics*, **39**, 2127–2142.
- Smith, R., and Coauthors, 2010: The parallel ocean program (pop) reference manual ocean component of the community climate system model (ccsm) and community earth system model (cesm). *LAUR-01853*, **141**, 1–140.
- Srokosz, M., and H. Bryden, 2015: Observing the atlantic meridional overturning circulation yields a decade of inevitable surprises. *Science*, **348 (6241)**, 1255–1257.
- Stommel, H., 1961: Thermohaline convection with two stable regimes of flow. *Tellus*, **13 (2)**, 224–230.
- Toom, M. d., H. A. Dijkstra, W. Weijer, M. W. Hecht, M. E. Maltrud, and E. Van Sebille, 2014: Response of a strongly eddying global ocean to north atlantic freshwater perturbations. *Journal of Physical Oceanography*, **44 (2)**, 464–481.
- van Westen, R. M., and H. A. Dijkstra, 2023: Asymmetry of amoc hysteresis in a state-of-the-art global climate model. *Geophysical Research Letters*, **50 (22)**, e2023GL106088.
- Van Westen, R. M., and H. A. Dijkstra, 2024: Persistent climate model biases in the atlantic ocean’s freshwater transport. *Ocean Science*, **20 (2)**, 549–567.
- van Westen, R. M., V. Jacques-Dumas, A. A. Boot, and H. A. Dijkstra, 2024a: The role of sea-ice processes on the probability of amoc transitions. *arXiv preprint arXiv:2401.12615*.
- van Westen, R. M., M. Kliphuis, and H. A. Dijkstra, 2024b: Physics-based early warning signal shows that amoc is on tipping course. *Science advances*, **10 (6)**, eadk1189.
- van Westen, R. M., E. Y. P. Vanderborght, M. Kliphuis, and H. A. Dijkstra, 2024c: Substantial risk of 21st century amoc tipping even under moderate climate change. *arXiv preprint arXiv:2407.19909*.
- Weijer, W., W. Cheng, O. A. Garuba, A. Hu, and B. Nadiga, 2020: Cmp6 models predict significant 21st century decline of the atlantic meridional overturning circulation. *Geophysical Research Letters*, **47 (12)**, e2019GL086075.
- Weijer, W., and Coauthors, 2019: Stability of the atlantic meridional overturning circulation: A review and synthesis. *Journal of Geophysical Research: Oceans*, **124 (8)**, 5336–5375.

- Wolfe, C. L., and P. Cessi, 2010: What sets the strength of the middepth stratification and overturning circulation in eddying ocean models? *Journal of Physical Oceanography*, **40** (7), 1520–1538.
- Wolfe, C. L., and P. Cessi, 2011: The adiabatic pole-to-pole overturning circulation. *Journal of Physical Oceanography*, **41** (9), 1795–1810.
- Wolfe, C. L., and P. Cessi, 2015: Multiple regimes and low-frequency variability in the quasi-adiabatic overturning circulation. *Journal of Physical Oceanography*, **45** (6), 1690–1708.
- Yang, K., H. Yang, and Y. Li, 2024a: A theory for self-sustained multicentennial oscillation of the atlantic meridional overturning circulation. part ii: Role of temperature. *Journal of Climate*, **37** (3), 913–926.
- Yang, K., H. Yang, Y. Li, and Q. Zhang, 2024b: North atlantic ocean–originated multicentennial oscillation of the amoc: A coupled model study. *Journal of Climate*, **37** (9), 2789–2807.
- Yeager, S. G., and J. Robson, 2017: Recent progress in understanding and predicting atlantic decadal climate variability. *Current Climate Change Reports*, **3**, 112–127.
- Zhang, R., R. Sutton, G. Danabasoglu, Y.-O. Kwon, R. Marsh, S. G. Yeager, D. E. Amrhein, and C. M. Little, 2019: A review of the role of the atlantic meridional overturning circulation in atlantic multidecadal variability and associated climate impacts. *Reviews of Geophysics*, **57** (2), 316–375.
- Zhu, C., and Z. Liu, 2020: Weakening atlantic overturning circulation causes south atlantic salinity pile-up. *Nature Climate Change*, **10** (11), 998–1003.